Integrated assessment of the hydraulic and structural performance of the OBREC device in the Gulf of Naples, Italy

Integrated assessment of the hydraulic and structural performance of the OBREC device in the Gulf of Naples, Italy

Giuseppina Palma[1], Pasquale Contestabile[2,3], Barbara Zanuttigh[1,3], Sara Mizar Formentin[1] and Diego Vicinanza[2,3,4]

1 Department of Civil, Chemical, Environmental and Materials Engineering, University of Bologna, Viale Risorgimento 2, 40136 Bologna, Italy; giuseppina.palma2@unibo.it, saramizar.formentin2@unibo.it, barbara.zanuttigh@unibo.it

2 Department of Engineering, University of Campania, via Roma 29, 81031 Aversa, Caserta, Italy; pasquale.contestabile@unicampania.it, diego.vicinanza@unicampania.it

3 Inter-University National Consortium for Marine Sciences (CoNISMa), 00196 Roma, Italy

4 CNR-INM, Institute of Marine Engineering, Via di Vallerano 139, 00128 Roma, Italy

Abstract

The aim of this work is to analyze the performance of the Overtopping Breakwater for Energy Conversion (OBREC), developed by the team of the University of Campania and installed at prototype scale in the port of Naples. It is a multifunctional coastal structure aimed to protect harbors and produce energy, based on the overtopping principle. This device has been preliminary analyzed by means of experimental and numerical investigations.

This contribution provides for the first time an integrated assessment of the OBREC hydraulic and structural performance, by means of the measurements collected at the prototype installation and of numerical modelling i.e. methodologies not affected by the scale effects. The numerical model, developed in the openFOAM environment, is calibrated on the field data gathered during a storm event and is then applied to extend the information related to the OBREC response under the typical wave climate. The results obtained are proposed in terms of overtopping discharge rates and pressures acting along the OBREC profile, under several sea states.

Based on these results some recommendations and indications regarding the optimal cross section design are given to maximize the energy production, without compromising the structural stability, and to promote the device exploitability.

1. Introduction

More than the 50% of the shoreline of Europe, US, Australia, and Asia has been modified by hard engineering, including groins and breakwaters to protect against erosion and wave action in support of recreational boating and other activities [14]. The shorelines are also facing more frequent and severe extreme events, increasing the financial costs of maintaining these structures under future climate change scenarios [23[45].

Recently, to counter this situation, a series of integrated approaches have been developed to preserve the ecosystems, minimize the social and the environmental impacts. Some examples are represented by eco-compatible sediment management for beach maintenance, a. o. “Sand Engine”, “Mud Motor” and beach drainage [9[36]. Other interventions provide ecosystem enhancement through the restoration and/or creation of habitats, such as sand dunes [22[29], saltmarshes restoration [17] or

intertidal buffer areas; actions to reduce the impact on society and economy including insurance frameworks, risk communication and landscape planning. Furthermore, new designs of breakwaters and dikes have been developed to combine coastal protection with leisure activities, such as artificial reefs and promenades [34], or with the production of marine renewable energy [28[42]. Their principal aim is to improve the use of coastal areas, while minimizing the installation/maintenance costs [1].

Specifically, in the framework of the energy production by means of Wave Energy Converter (WEC) devices, two promising technologies have been designed to be entirely embedded into traditional coastal defence structures to share the costs, i.e. Oscillating Water Column (OWC hereafter) and the Overtopping Device (OTD hereafter) [42]. The former is capable of harvesting energy from the oscillation of the seawater inside a semi – submerged chamber, while the latter collects the seawater of incident waves in a reservoir above the sea level, then released by means of turbines. Both of them are concrete – made devices, which can be placed or integrated in new or existing breakwaters, aimed to i) protect the harbour inshore area, and ii) produce energy.

Some prototype of OWCs exist, such as the REWEC3 [3], the PICO [33], the LIMPET [2] and the MUTRIKU [37] power plants. The first onshore OTD device, i.e. the Slot Sea Cone Generator [43], consisted of a concrete dike with multiple reservoirs, suited for a wide spectrum of different wave conditions. However, this technology resulted to be economically unfeasible due to its complex geometry. Starting from this experience, the team of the University of Campania developed a new Overtopping Breakwater for Energy Conversion, OBREC hereafter [41]. It is a traditional rubble mound breakwater including a top concrete structure, i.e. the device that consists of a ramp followed by a reservoir closed by a crown wall. The reservoir is located above the still water level and it is linked with the machine room by means of a pipe passing through the crown wall. The potential energy of the overtopping waves collected inside the reservoir is converted by means of low – head turbines in the machine room.

OBREC was preliminary investigated under ordinary and extreme wave conditions by means of both small-scale experiments [41] and numerical modelling [31[32] to support the design of the prototype installed in the port of Naples. During the autumn-winter 2016/17, a first rough monitoring campaign was performed to observe the OBREC functioning under a real sea state and to check if the energy conversion occurred in safe conditions [10]. To provide more detailed information about the wave-structure interactions, a second monitoring campaign was carried-out between Autumn 2017 and Spring 2018, in the context of the project BRIGAID (Bridging the Gap Innovations in Disaster Resilience) (https://brigaid.eu/), funded by the EU Horizon2020 program.

This paper aims to support and extend the information obtained from of this second field monitoring campaign by means of 2D numerical modelling. Section 2, presents the pilot plant, the monitoring system, the storm events recorded at the beginning of the 2018 used to calibrate the numerical model and the wave conditions characterizing the typical wave climate at the installation site, used to analyse the integrated response of the device. Section 3 is dedicated to the numerical modelling set-up, including the description of the model, the implemented wave conditions, the characteristics of the structure and the numerical domain and the numerical measurements performed. Section 4 compares the numerical results with the field data acquired during a real single storm event, focusing on the structural response of the device. Furthermore, in Section 5, the same model has been adopted to provide an integrated assessment of the structural and the hydraulic performance of the OBREC device under the typical wave climate of Naples. Based on these results, Section 6 gives some

recommendations and indications about the optimal design of the OBREC geometry to maximize the energy production.

2. OBREC pilot plant

2.1 Description of the prototype installation

The first OBREC pilot plant was installed at the end of 2015 in the existing San Vincenzo breakwater, which protects the Port of Naples (Italy) in the Middle Tyrrhenian Sea. The geographical coordinates of the site are 40° 49’ 58.68’’ N and 14°16’ 03.64’’ E (Fig. 1), which resulted to be ideal for a first installation, due the following reasons:

- the low-occurrence of extreme events, which allows a safety installation and maintenance procedures;
- the principal direction of the waves is quasi orthogonal with respect to the device, leading to perform a 2D numerical investigation;
- the non-breaking wave conditions, thanks to the 25 m water deep at the toe of breakwater;

The San Vincenzo breakwater is a traditional rubble mound breakwater, provided with an external layer made of artificial concrete blocks (the so called “Antifers”, i.e. grooved concrete with holes), a filter layer made of rocks (characterized by different diameters) and a quarry run core. The actual offshore slope can be approximated at 1:2. However, the random placement of the Antifers created a curved profile, which acts like a berm due to the combination of the relative water depth and typical higher waves at the site. A road, located at the rear side of the structure, allows the access to the breakwater (Fig. 1), simplifying the construction and maintenance operations and reducing the costs with respect to offshore installations.

The general cross section of the device consists of a ramp, which improves the run-up process, followed by a reservoir-crown wall system, collecting the overtopping waves. The latter is linked, by means of a pipe, with the machine room hosting the turbines. The crown wall, aimed to protect the inshore area, is provided with a parapet on top of it to reduce the overtopping discharge at the rear side of the structure. The overall installation has a crest level of 4.50 m above the still water level (SWL in Fig. 1).

The structure was cast in-situ, except for the prefabricated ramps, and placed directly on the external layer. However, to enhance the overall stability, the foundation involved the installation of 12 concrete micropiles constituted by steel tubular reinforcement with an external diameter of 300 mm, and thickness of 25 mm and a total length of 10 m.

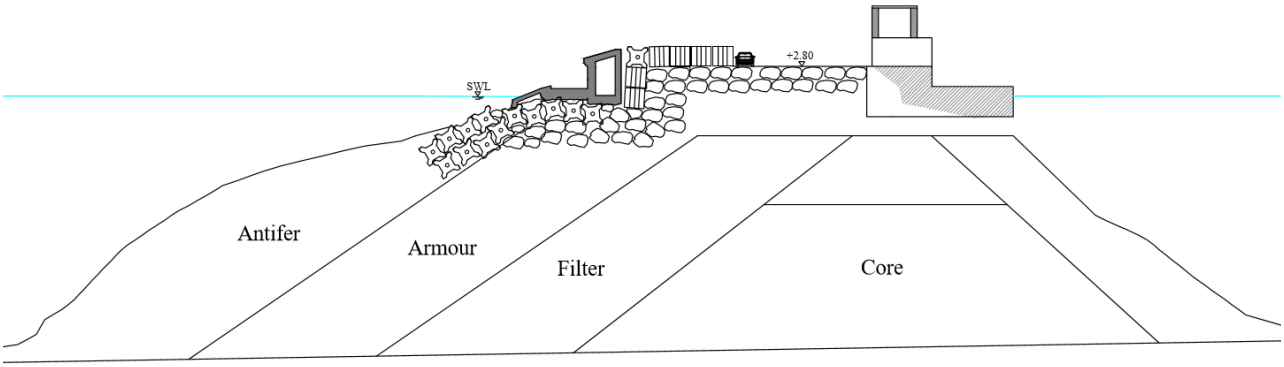

Fig. 1. Location of the pilot plant in the middle of the San Vincenzo breakwater (Port of Naples. Italy).

The prototype is composed by 2 configurations, divided by a wall septum, which differ for the height of the ramp, i.e. R_c. Specifically, the RS-LAB (*Real Scale laboratory*) and the NW-LAB (*Natural Waves Laboratory*) cross sections are characterized by a ramp 2.0 m and 1.2 m high, respectively (values referred to the mean tide level, see Fig. 2). In both cases, this parameter was tuned on the typical wave climate characterizing the installation site. In particular, the NW-LAB is intended to capture the mean run-up of the most frequent waves (i.e. H_s = 0.75 m, see Table 1), while the RS-LAB refers to the higher energetic sea states and operative consideration about the nominal hydraulic head of commercial low-head Kaplan turbines, i.e. about 1.5-2 m [32]. The ramp includes a double inclination of 78° and 22°, according to the field observations and to the results obtained from the numerical investigations performed by Palma et al. [32]. The submerged quasi-vertical part of the ramp was introduced to i) improve its resistance to bending and fatigue, and to ii) enhance the stability of the device placed on the armour layer.

The whole installation has the same longitudinal dimension, i.e. from the beginning of the ramp to the inshore edge of the machine room. The common parts for both the configurations are i) the rear crown wall, provided with a bullnose, and ii) the machine room (6.0 m x 3.4 m). According to this spatial constraint, the reservoirs have different dimensions, i.e. 2.5 m and 3.65 m for the RS-LAB and NW-LAB (see Fig. 2), respectively. The wider reservoir is associated to the lower ramp, which is the more frequently overtopped, and vice versa. Indeed, the experimental and numerical investigations performed by Iuppa [24] and Palma [32]**,** respectively, demonstrated that the selection of the reservoir longitudinal width can be subordinated to the height of the ramp. This latter parameter has to be tuned on the specific wave climate and directly affects the overtopping volumes and, therefore, the hydraulic performance. The reservoir is linked with the machine room by means of pipes passing through the crown wall. The RS-LAB is provided with two pipes of 0.25 m of diameter, while the NW-LAB has also a third one of 0.17 m of diameter (see Fig. 3a and 3b). At this stage, the flow for both the configurations is passing through the biggest pipe only, which is located in the lowest position (Fig. 3b, 3c). The other pipes will give the chance to test the effects on both the power production and on the loadings on the crown wall induced by the use of more than one pipe contemporarily and by the different locations of the openings.

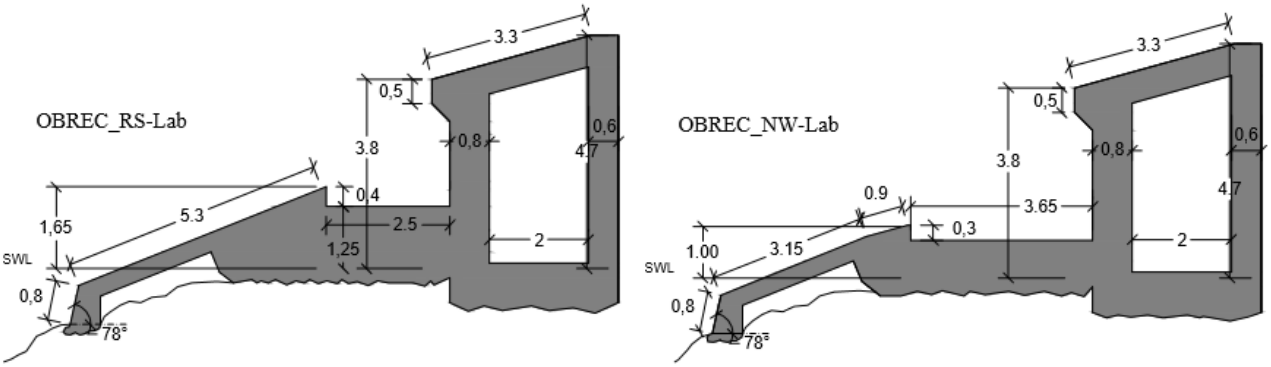

Fig. 2. Cross-sections of the OBREC prototype configurations in the Naples harbour: a) RS-Lab configuration; b) NW-Lab configuration [10].

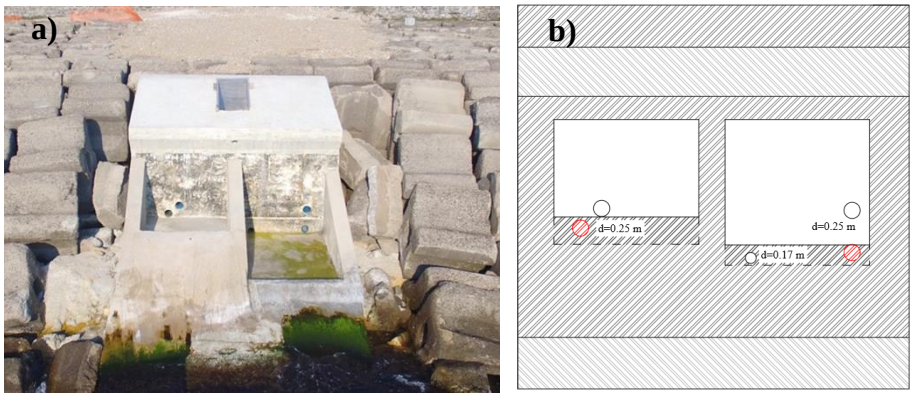

Fig. 3. a) Frontal view of the OBREC prototype installed in the port of Naples, and b) position of the pipes (in red the open ones).

2.2 Field Monitoring Campaign: equipment and measurements

The pilot plant is provided with several instruments to gather information both on the wave conditions and the hydraulic and structural response of the structure. A GPS wave buoy, the Directional Wave Spectra Drifter (DWSD), is located 100 m far from the San Vincenzo breakwater, in front of the OBREC device, i.e. latitude 40°49'57.68" – longitude 14°16'3.43". The DWSD buoy was provided by the Scripps Institution of Oceanography (https://scripps.ucsd.edu/). It uses the GPS sensor package in order to measure *w(t)*, *u(t)* and *v(t)*, which represent respectively the vertical, horizontal E-W and the horizontal S-N buoy velocity components [6]. These data are acquired from the changes in the frequency of the GPS signal. The sampling of *u(t)*, *v(t)* and *w(t)*, acquired at 1 Hz, is performed for 17 min every hour, and the main wave data parameters are transmitted in real-time through the Iridium satellite system. The information related to the wave conditions are accessible on a dedicated website together with the battery voltage and pressure, the temperature and humidity of the hull. The DWSD-buoy located in front the pilot plant, is shown in Fig. 3.

To assess the hydraulic performance, the water flowing through the pipes is collected in a shunt tank, located in the machine room. Inside the tank, a resistive gauge measures the hydraulic head with an acquisition frequency of 10 Hz, with the purpose of optimising i) the position/dimension of the pipe, and ii) the design of the shunt tank, considering the typical wave climate. When an overflow occurs, the excess water is driven back to the sea by means of a specific overflow discharge.

To measure the pressures acting on the device, 3 pressure transducers were installed on the RS-LAB ramp, i.e. F, G and H in Fig. 5; and 4 along the NW-LAB crown wall and in correspondence of the

bullnose, i.e. A, B, C and N in Fig. 6. Their characteristics were selected according to the expected hydrodynamic loads, which were measured and analysed during the small-scale laboratory campaigns performed by Contestabile [11]. Specifically, these transducers can measure the pressures ranging from 0 to 100 bar, with a full scale F.S. precision at 25° of 0.4%, under a temperature range from - 40° to 125°. The output signals vary between 4 and 20 mA. Although the original acquisition frequency is 1 kHz, the signal was instantaneously low filtered to 100 Hz, by keeping the maximum value of 10 consecutive measures. This procedure reduces the amount of the gathered data, without losing information about the highest loads.

Fig. 4. The DSWD located in front of the OBREC prototype.

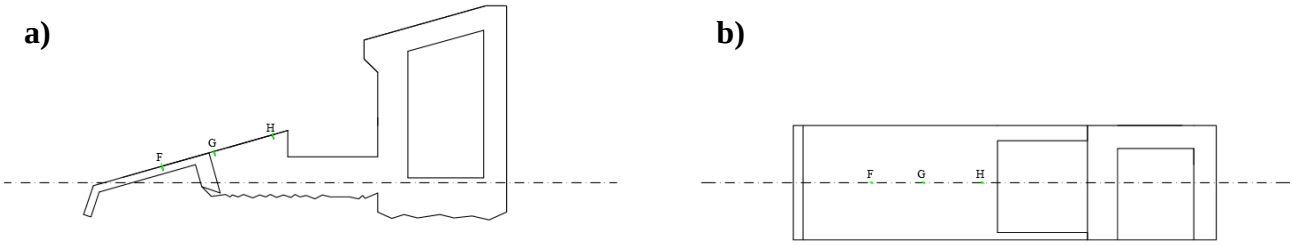

Fig. 5. a) Longitudinal and b) flat sections of position of the pressure transducers for the RS-LAB configuration.

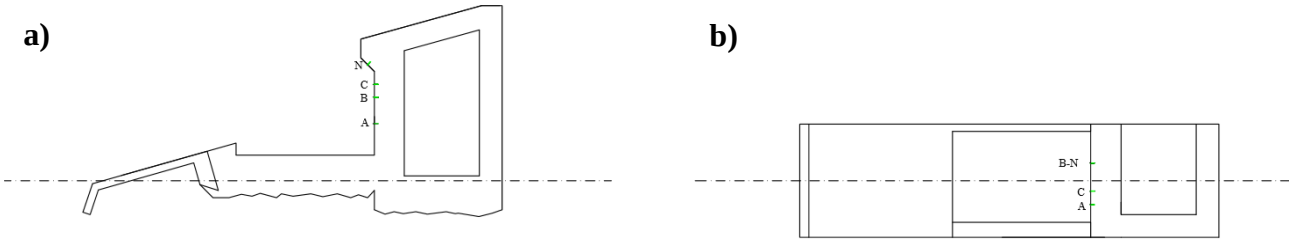

Fig. 6. a) Longitudinal and b) flat sections of position of the pressure transducers for the NW-LAB configuration.

Fig. 7. Pressure transducers installed on the OBREC device.

2.3 Wave climate at the pilot plant

Due to the short period of wave monitoring with the DWSD buoy, the typical wave climate in front of the OBREC has been calculated by propagating the hind cast data from the European Centre for Medium-Range Weather Forecasts (ECMWF) collected offshore the Gulf of Naples during the period 2006-2016.

For studying the long-term variation of the wave height, the use of the ERA-Interim dataset could be considered adequate, i.e. reliable and generally slightly conservative for wave energy assessment [13]. The mean wave power was found to range between 1.6 and 2.5 kW/m. Table 1 shows the wave climate corresponding to an average year (yearly mean wave energy density of 1.87 kW/m). In particular, the typical wave climate is reconstructed by means of 8 sea states (Table 1), which are characterized by a significant wave height H_s (i.e. the average height of the highest one-third of all the measured waves), a mean period T_m (i.e. the mean of all the wave periods in a time-series representing a certain sea state) and a certain frequency of occurrence Fr during the year. The wave properties determine the energy flux P_{abs} per unit of wave – crest length, defined in Eq. (1):

$$P_{abs} = \frac{\rho g}{64} T_m H_s^2 \frac{1}{1000} \tag{1}$$

where ρ is the water density and g is the gravitational acceleration. By multiplying P_{abs} by the values of Fr, it is possible to obtain the annual contribution of the theoretical wave energy flux per unit length P_{year}, given by each sea state as reported in Table 1, by neglecting all the losses.

Table 1. Characteristics of the wave conditions of the typical climate of Naples.

Sea states	H_s [m]	T_m [s]	P_{abs} [kW/m]	Fr [%]	P_{year} [kW/m]
1	0.25	2.25	0.06	0.1498	0.01
2	0.75	3.90	1.01	0.5912	0.60
3	1.25	5.03	3.61	0.2083	0.76
4	1.75	5.95	8.37	0.0409	0.34
5	2.25	6.75	15.68	0.0083	0.14

6	2.75	7.46	25.90	0.0012	0.02
7	3.25	8.11	39.33	0.0003	0.01
8	3.75	8.71	56.25	0.0001	0.01

2.4 Storm conditions in the monitoring period

During the first semester of 2018, 5 storm events with a quasi-orthogonal wave direction were recorded by the DWSD buoy. Table 2 reports the dates, the duration, the storm duration-averaged significant wave heights $H_{s,mean}$, the maximum significant wave heights $H_{s,max}$, and the mean period T_m. These storm events correspond to typical winter storms in the study site (i.e. expected to have from 1 to 2 years return period). As anticipated, the original acquisition frequency is 1 kHz, instantaneously low-filtered to 100 Hz. Although this procedure strongly reduced the amount of data, the elaboration of the raw signals required a huge effort. The procedure is tuned on the first available storm event S1, which is then selected to be reproduced in the numerical model.

The storm S1 (see Table 2) is characterized by a rising phase during the first 2 days, a peak phase of 6 h and a decay phase that lasted up to 2 days) (see Fig. 8).

The field and numerical data were compared at the peak phase to focus the analysis on the most severe part of the storm event. Indeed, it is characterized by $H_{s,mean}$ = 2.13 m and T_p = 8.37 s, used as input parameters to describe the wave attack in the numerical simulations. In both the cases, physical and numerical testing, the response of the structure is determined by measuring the pressures exerted by the wave attack along the OBREC profile. The results obtained have been synthetized by computing the maximum pressures p_{max} and the statistical representative values such as p_{250} and p_{100}, which represent the non-exceedance values of 99.7% and 90% respectively.

Table 2. Storm events occurred at the beginning of the 2018, characterized by a mean period Tm and a storm duration-averaged significant wave heights, $H_{s,mean}$, and a maximum significant wave heights $H_{s,max}$, respectively.

Storm event	Date	Duration [days]	$H_{s,mean}$ [m]	$H_{s,max}$ [m]	T_m [s]
S1	(6 – 10)/1/2018	5	1.99	2.47	5.58
S2	(15 – 18)/1/2018	4	1.72	2.02	5.20
S3	(1 – 4)/2/2018	4	1.98	3.07	5.85
S4	(20 – 22)/3/2018	3	1.93	2.21	5.52
S5	(31 – 2)/4/2018	3	2.47	2.81	6.36

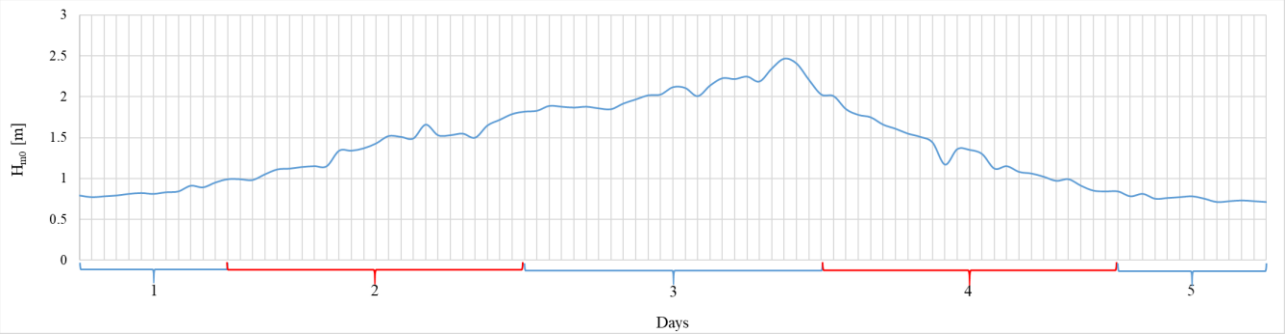

Fig. 8. Variation of the significant wave height H_s during the storm event S1, described in Table 2. Measurements derived from DSWD located in front of the OBREC prototype (see Fig. 4).

3. Set-up of the numerical model

3.1 Overview of the numerical model

The 2D numerical simulations have been performed with the free, open source CFD software openFoam (www.openfoam.org). Specifically, the toolbox *waves2Foam*, originally developed at the Technical University of Denmark by Jacobsen et al. [25] and capable of generating/absorbing the waves, has been used.

The principal direction of the waves in the installation site is mainly perpendicular to the OBREC device all over the year. Therefore, this reduces the error due to simulating the wave – structure interactions of the real site by means of a 2DV representation. The model is based on the Volume Average Reynolds Average Navier Stokes equations (VARANS), implemented using the (Volume of Fluid) VOF method. The library *waves2foam* is a modification of the native one, i.e. *interFoam*. It is capable of solving 2 incompressible, isothermal immiscible fluids, i.e. air and water, simultaneously tracked using the scalar field γ (equal to 0 for air and 1 for water, and any intermediate value is a mixture of the two fluids), considering the wave generation/absorption by means of the relaxation zone technique In the momentum balance equation, an extra term is included to take into account of the surface tension between the two phases. The generation/absorption of free surface water waves is based on the application of the relaxation zone technique (active sponge layers), and includes a large range of wave theories for regular and irregular waves.

The turbulence Large Eddy Simulations (LES) model [7] has been introduced for this study case, since the Direct Numerical Simulation (DNS) approach, in which the full Navier–Stokes equations are numerically solved directly from the smallest to the largest eddies, would be computationally too expensive. On the other hand, the Reynolds-averaged Navier–Stokes (RANS) approach solves only the averaged quantities and it is therefore used when it is not necessary to simulate the detailed instantaneous flow. The LES approach computes directly the large-scale motions (large eddies) of turbulent flow, while models only the small-scale [46]. Therefore, it has been preferred because it enormously reduces the computational cost with respect to DNS, being more accurate than RANS.

The geometries, the numerical domain and the mesh have been defined, at prototype scale, by means of Gmsh [21], a free 3D finite element mesh generator with a built – in CAD engine and post – processor.

The characteristics of the PC used to simulate the wave conditions are reported in Table 3, here below:

Table 3. Characteristics of the PC used to simulate the wave conditions.

Ubuntu version	14.04 LTS
Memory	31.2 GiB
Processor	Intel Xeon(R) CPU ES-2690 v3@2.6 GHz x 16
Graphics	Gallium 0.4 on NVE7
OS type	64 bit
Disk	1.9 TB

3.2 Wave attacks

The OBREC response is analyzed i) during a monitored storm event, and ii) under the typical wave climate of Naples. Therefore, the following wave attacks were selected:

- storm wave condition: a time window of 6 h is selected from the whole S1 data series. It is centered around the peak phase (i.e. 3 h before and 3 h after), characterized by significant wave height H_s = 2.13 m and a peak period T_p = 8.37 s;
- typical wave conditions: a sub–set of wave conditions is used to assess the hydraulic and structural performance of the OBREC under the typical wave climate (Table 1). Each wave attack lasted in this case for or about 600 waves.

The wave attacks were reproduced by implementing a Jonswap wave spectrum characterized by a peak enhancement factor γ_P = 3.3.
In order to ensure a suitable number of waves for a reliable statistical analysis, i.e. 600 waves [35], the length of the simulations vary according to the sea state and, specifically, according to the peak period. Therefore, the runtime of simulations is in the range of 1-2 weeks, for the shortest (sea state 3 in Table 1) and the longest (sea state 8 in Table 1) simulations, respectively.

3.3 Characteristics of the tested cross sections

The 2 cross sections composing the OBREC prototype, have been tested separately. Hence, two numerical model, representing half of the structure (see Fig. 9), have been defined. This allowed to drastically reduce the numerical domain, minimizing the computational effort without compromising the interactions between waves and porous media. Indeed, an open-flow condition and an absorption relaxation zone (Fig. 9), is implemented as the outlet boundary, to support the free outflow of the water. The porous layers, composing the San Vincenzo breakwater, are characterized by a cell size equivalent to the nominal diameter of the rocks. In *waves2foam*, the flow through the porous media is modelled by means of the extended Darcy-Forchheimer equation [19]. The term related to the turbulent flow follows the expression developed by Van Gent [40], representing the effect of the oscillatory flows through the Keulegan-Carpenter (KC) number.

$$b = \beta\left(1+\frac{7.5}{KC}\right)\frac{1-n}{n^3}\frac{1}{gD_{50}} \tag{2}$$

The parameters needed to characterize a specific layer are: porosity n [18]; added mass coefficient c_A [40]; KC number, linear and non-linear friction coefficients α and β. These parameters have been set based on the sensitivity study performed by Jensen et al. [26] on a traditional rubble mound breakwater, similar to the structure involved in the present study case, see Table 4. Furthermore, they have been selected by calibrating them against the measured pressure data, to obtain an overall reliable estimation of the loads acting along the OBREC profile.
The offshore slope, composed by Antifers, is represented as a straight line (Fig. 9). In the reality, the random placement of the concrete blocks produced a curved edge, which acts like a berm. This simplification has to be taken into account during the analysis of the numerical results.

Table 4. Characteristics of the porous layers composing the San Vincenzo breakwater.

	n	KC	c_A	D_{50} [m]	α	β
Antifer	0.50	128	0.34	2	500	2.0
Armour	0.45	128	0.34	1.4	500	2.0
Filter	0.45	128	0.34	0.75	500	2.0

Core	0.45	128	0.34	0.50	500	2.0

The OBREC configurations have been numerically tested by means of 2D simulations, which represent a good approximation of the real case since that the main wave direction is orthogonal to the prototype installation.

To analyze the OBREC behavior under the typical wave climate, the two configurations were provided with a pipe with the same nominal dimension of the prototype. However, due to the limitation of the 2D model, the pipe is modeled as a rectangular hole covering the whole width of the domain. Test cases with open pipe conditions are referred hereinafter as “open”.

For the analysis of the selected storm event, an additional case is proposed, by closing the pipe (“closed” in the following), to represent the most severe conditions, corresponding to the prototype observation that the reservoirs do usually work in saturated conditions during severe storms.

3.4 Numerical wave flume and mesh

The numerical domain is defined considering the extreme wave condition, i.e. Test 8 in Table 1, to correctly represent the wave development for all the sea states considered.

The length of the domain is set equal to 334 m, which corresponds to 3 times the wavelength L = 107.5 m. It includes an inlet relaxation zone for the wave generation, which has to be at least half of the wavelength (i.e. 54 m), followed by two wavelengths (i.e. 215 m) to let the wave to be completely developed before reaching the structure (Fig. 9). The breakwater footprint length is 65 m (see Fig. 11), including the outlet relaxation zone (10 m).

The wave height affects the extension of the vertical dimension of the domain. To minimize the computational effort, i.e. the number of the cells, the domain is divided in 2 parts, which differ for their vertical extension and for the mesh adopted. The first part is 31 m high, i.e. 26 m of water depth plus 5 m to allow the correct representation of the waveform. In the second part, where the wave – structure interaction occurs, the vertical dimension is extended up to 35 m.

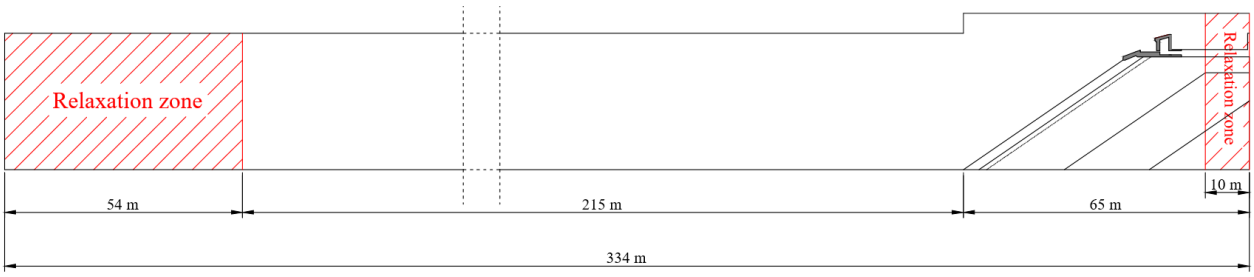

Fig. 9. Scheme of the numerical domain.

The mesh characterizing the first part of the domain is structured and graded, both in the horizontal and vertical directions (Fig. 10). In particular, the cell dimension decreases in correspondence of the still water level and going towards the structure. The second zone is characterized by an unstructured mesh, more flexible and suitable for peculiar geometries, i.e. the OBREC device installed in a traditional breakwater. The grid reaches its minimum dimension, i.e. 0.02 m, in correspondence of the reservoir and the pipe inside the OBREC, where a high accuracy of the results is required (Fig. 11). The mesh here described has been adopted for all the tested wave conditions. In the worst case, i.e. sea state 3 in Table 1, during the wave propagation the discretization is

$L/\Delta x \approx 100$ and $H_s/\Delta y \approx 10$. The latter ratio, due to the refinement performed in correspondence of the structure becomes $H_s/\Delta y \approx 60$, to better represent the wave-structure interaction.

The bottom edge of the numerical domain has been set as impermeable. The left and the right edges are combined with the inlet and outlet relaxation zones. The former is responsible of generating the wave trains, while the latest allows the free outflow of incoming water, taking into account also of the presence of the porous media. The atmosphere patch characterize the top edge and the end of the pipe, to let the fluids to freely flow out of the domain.

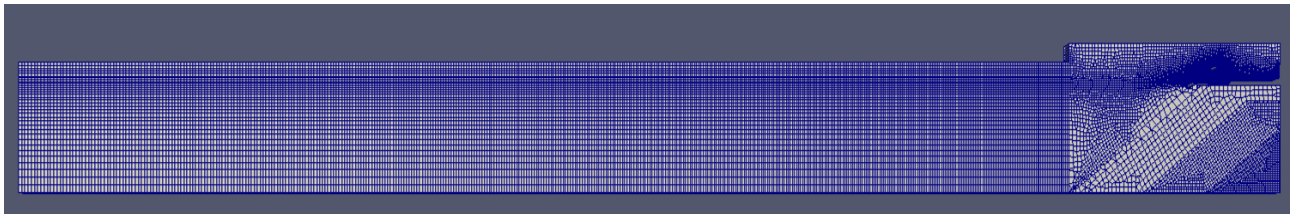

Fig. 10. Mesh characterizing the numerical domain.

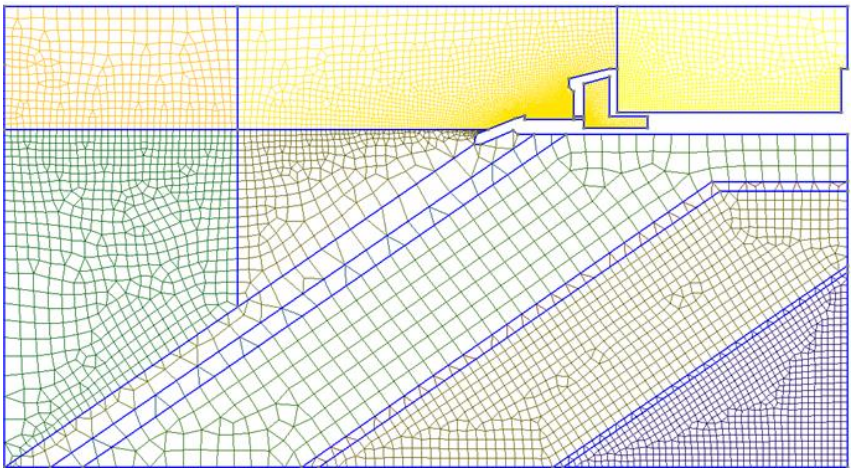

Fig. 11. Unstructured mesh characterizing the second part of the domain, occupied by the breakwater.

3.5 Numerical Measurements

Several wave gauges and probes are placed inside the numerical channel and along the structure to analyze the surface elevations, the velocities profiles and the pressures acting on the device. The general output Time Step and the Courant number are equal to 0.1 s and 1, respectively, for all the simulations. However, the sampling frequency of the pressures, performed during the runtime, has been forced to 100 Hz, to be consistent with the field data acquisition.

To track the free surface location, 35 wave gauges are set every 10 m from the beginning of the domain until the structure toe. The wave reflection coefficient K_r is evaluated, applying a 3-point method [27] to the 3 gauges positioned at 155, 156.1 and 157.8 m, about 2 wavelengths L far from the structure.

The average overtopping discharge rates inside the reservoir Q_{in}, flowing through the pipe Q_{pipe} and overtopping the rear side of the structure Q_{rear} (Fig. 12) have been computed by integrating the horizontal water velocity components along the vertical direction. The velocity output is given every 0.005 m inside the pipe, while is discretized every 0.01 m at the rear side of the structure and inside the reservoir. The different accuracy is to achieve the best representation of the different dynamics related to these 3 parts of the structure.

In order to have a more comprehensive understanding of the OBREC functioning under the typical wave climate, an additional parameter has been computed, i.e. $T_{\%,full}$. It represents the average percentage of the pipe section filled by water, during the entire simulation. Fig. 12 shows the location of the pressure measurement points along the OBREC profile. A linear pressure distribution between two consecutive transducers has been assumed along the structure, considering the short distance between the probes, i.e. 0.02 m along the entire profile, except for the probes related to the uplift pressures.

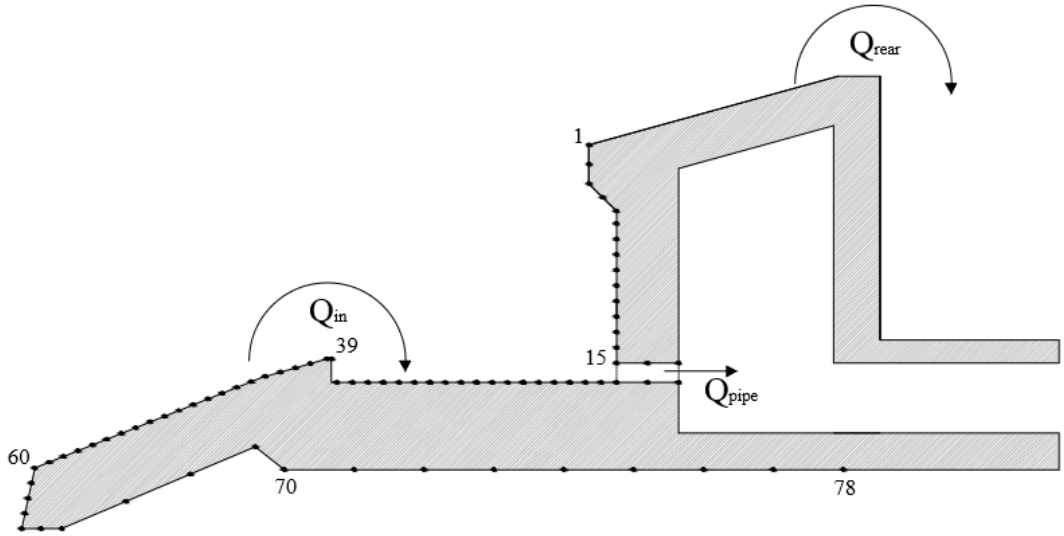

Fig. 12. Example of the measuring points for the NWLAB configuration, i.e. pressure probes and discharge rate inside the reservoir Q_{in}, through the pipe Q_{pipe} and at the rear side of the structure Q_{rear}.

4. Results

4.1 Numerical and observed wave loading under a storm

The results for the two numerical OBREC configurations are directly compared with the pressures measured during the peak phase of the storm event S1 (see Table 5), by the transducers installed on the OBREC prototype (see Fig. 6). The results are here proposed in terms of maximum and statistical values, p_{max} and p_{250} in Table 5. The latter one corresponds to the non-exceedance level of about 99.7% (i.e. the average of the highest 4% of values).

Table 5 shows that the numerical model tends to generally overestimate the field data, except for the upper part of crown wall of the open configuration, i.e. pressure transducers C and N. This is due to the 2D representation of the pipe that covering the entire width of the numerical domain absorbs part of the overtopping waves. In a 3D representation, the continuity of the wall would enhance the wave run-up, increasing the maximum pressures acting on the upper part of the crown wall and against the bullnose (see the values pf p_{max} of C and N in Table 5 related to the closed configuration). Therefore, the monitored p_{max} are expected to fall in the middle of these two cases, i.e. open and closed reservoirs. However, the numerical values of p_{250}, which are more representative than p_{max} for the purposed of a fatigue analysis, show a good agreement with the field measurements, while they result in a cautious estimation along the OBREC profile even if the solver does not take into account of the compressibility of the fluids.

The numerical values of p_{max} and p_{250} on the ramp are about 4 times higher than the monitored ones (Table 5). These differences could be related to the following main simplifications:

- the wave spectra were sampled by the DWSD buoy with a frequency of every 17 to 60 min and, therefore, it is impossible to perfectly replicate the wave profile by the numerical model;
- the offshore slope of the external layer is represented as a straight line. In the reality, the random placement of the blocs created a curved edge (see Fig. 1), which acts like a berm, anticipating the local breaking process;
- the ramp is numerically represented as completely in-built on the breakwater, while in reality it is placed on the Antifers blocks (Fig. 13), leading to significant change in the representation of the flow under the plate and of the resulting lift force on the device;
- numerical simulations are observed to generate lower level of run-down and more noisy pressure signal, with higher spikes compared to the physical tests, according to a previous study on the Seawave Slot-cone Generator [5];
- the effect of air, not modeled in the numerical model, have some influence on the correct representation of impact waves series, as also found by Di Lauro et al. [15]. In particular, the oscillatory nature of the pressure signals is influenced by the compression of the air-pocked trapped between the wave and the parapet, leading to a general overestimation in numerical model.

Table 5. Maximum and statistical pressure values p_{max} and p_{250} in kPa, measured during the monitoring compared with the numerical results related to both the open and closed OBREC configurations.

Probes	F	G	H	A	B	C	N
				p_{max} [kPa]			
Prototype	9.0	8.8	8.8	31.8	37.9	45.6	38.4
Open Conf.	20.1	21.2	29.5	71.5	47.2	30.5	36.2
Closed Conf.	25.6	27.1	30.8	78.1	85.6	70.7	62.7
				p_{250} [kPa]			
Prototype	5.0	4.8	4.8	17.9	21.3	25.6	21.7
Open Conf.	19.6	20.7	22.7	35.2	28.7	27.8	32.2
Closed Conf.	24.4	25.5	28.9	37.3	39.6	38.9	38.6

Fig. 13. Construction of the bottom slap and positioning of the prefabricated ramps.

The numerical model allows also a direct comparison between i) the NW-LAB and the RS-LAB configurations, and ii) the closed and the open cases. Fig. 14 and Fig. 15 show qualitatively the pressures, i.e. p_{max} and p_{250}, acting along the open and closed cross sections during the storm S1, for the NW-LAB and RS-LAB cases, respectively. Main results can be summarised as follow:

- p_{max} and p_{250} shown similar qualitative distribution, especially for uplift and loading on the sloping ramp;
- NW-LAB results to be more stressed with respect to the RS-LAB configuration, because of the lower ramp that leads to a greater overtopping and less wave protection;
- the closed configuration provide higher pressures in the upper part of the crown wall;
- in the open case, the presence of the pipe, that limits the run-up along the crown wall, make the lower part and the reservoir more stressed;
- the pressure distribution along the ramp and the bottom edge of the device does not show a strong impulsive component as for the crown wall and the reservoir. This observation is supported also by the similarity between the maximum and the statistical values along these two parts of the structure;
- for the uplift pressures, the presence of contiguous porous layers, characterized by smaller diameters, going towards the inshore edge of the breakwater, damps the loads.

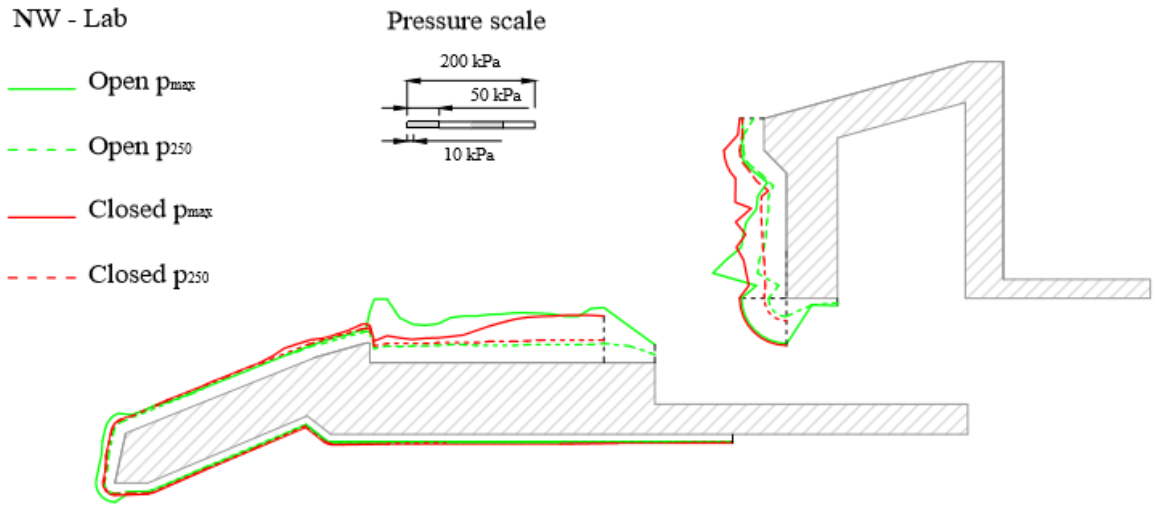

Fig. 14. Qualitative representation of the maximum and statistical pressures acting along the OBREC profile, during the numerically simulated storm event A, for NW-LAB configuration (open and closed cases).

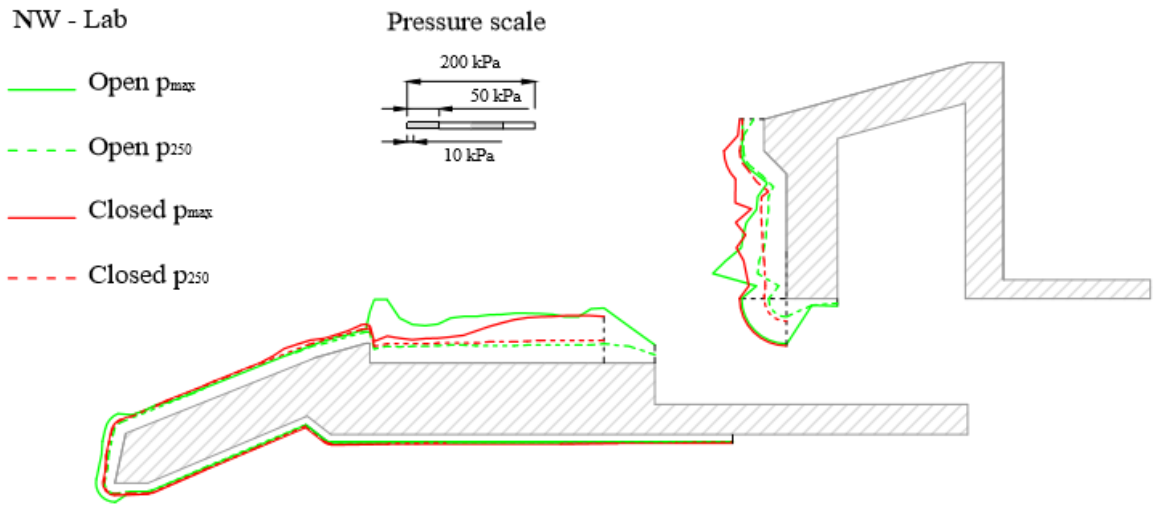

Fig. 15. Qualitative representation of the maximum and statistical pressures acting along the OBREC profile, during the numerically simulated storm event A, for RS-LAB configuration (open and closed cases).

4.2 Hydraulic and structural response under the typical wave climate

The hydraulic and structural performance of the OBREC under the typical wave climate are analysed to improve the OBREC design. These 2 technical aspects are fundamental in terms of energy production, but also of structural reliability. Indeed, the tested wave conditions were selected considering that the ratio H_s/R_c. had to be bigger than 1, i.e. sea state 3-8 for the NW-LAB and 4-8 for the RS-LAB configurations (Table 1). The purpose is to obtain interesting information in terms of overtopping and loads.

Table 5 reports the discharge rates flowing inside the reservoir Q_{in}, through the Q_{pipe} and at the rear side of the structure Q_{rear}. Furthermore, the values of K_r and $T_{\%,full}$, which represent the wave reflection coefficient and the percentage of time in which the pipe works in saturated condition, are presented. The values of Q_{in}, Q_{pipe} and $T_{\%,full}$ are strictly related to each other. By analysing the general trend, all these values increase with the increasing of H_s (see Table 6 and Fig. 16). Indeed, for the highest waves the pipe lose its capacity of absorbing all the water that goes inside the reservoir. However, the analysis of the values of $T_{\%,full}$ shows that the average percentage of filling of the pipe section, for the most severe wave condition here analysed, is the 62% and 48% for the NW-LAB and the RS-LAB case, respectively.

By comparing the 2 configurations the NW-LAB case shows, for all the sea states, higher values of Q_{in}, Q_{pipe} and $T_{\%,full}$ due to then lower ramp, which allows more overtopping with respect to the RS-LAB. However, further considerations are needed to define which is the most promising configuration. Indeed, the characteristics of the NW-LAB cross section (see Fig. 2) minimize the distance between the still water level and the theoretical position of the rotor of the turbine the theoretical position of the rotor of the turbine, at the expense of the theoretical energy production.

The values obtained of Q_{rear} in Table 6 respect the limits for wave overtopping for structural design of breakwaters, seawalls, dikes and dams suggested by the EurOtop [18]. Indeed, the presence of the parapet, on top of the crown wall, allows the minimization of the overtopping rate at the rear side of the structure [38[39], as already demonstrated during the preliminary experimental and numerical investigations [32[41].

The basic principle of the wave energy absorption, on which the OBREC has been designed, avoids the increasing of the values of K_r, with respect to traditional rubble mound breakwater, as already experience during the laboratory experiments performed by Vicinanza et al. [41].

Table 6. Discharge rate inside the pipe Q_{pipe} and at the rear side of the structure Q_{rear}, percentage of the time in which the pipe works as a full section and the reflection coefficient K_r for both the configurations.

H_s [m]	NW_LAB					RS_LAB				
	Q_{in} [m³/s]	Q_{pipe} [m³/s]	$T_{\%,full}$ [/]	Q_{rear} [m³/s]	K_r [/]	Q_{in} [m³/s]	Q_{pipe} [m³/s]	$T_{\%,full}$ [/]	Q_{rear} [m³/s]	K_r [/]
1.25	0.029	0.029	0.11	0	0.46	/	/	/	/	/
1.75	0.105	0.102	0.25	0	0.50	0.024	0.0226	0.07	0	0.51
2.25	0.221	0.170	0.35	0	0.46	0.107	0.09	0.19	0	0.46
2.75	0.411	0.296	0.57	0	0.47	0.238	0.193	0.35	0	0.50
3.25	0.629	0.364	0.59	0.0047	0.45	0.346	0.214	0.33	0.02	0.47
3.75	0.757	0.415	0.62	0.0053	0.48	0.484	0.324	0.48	0.0188	0.54

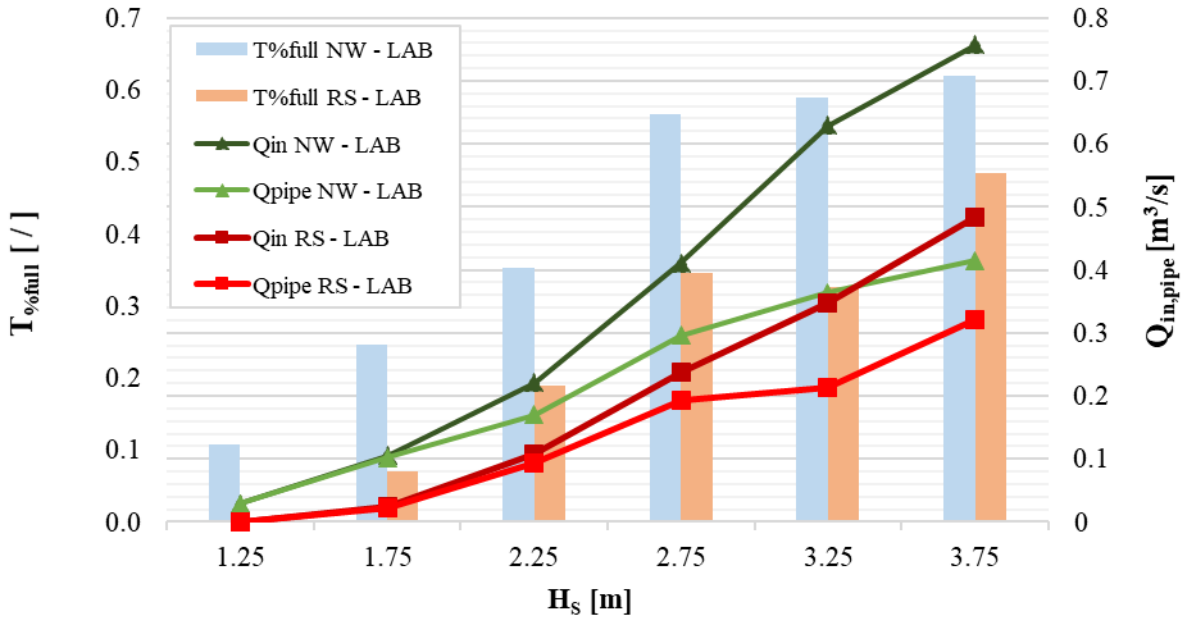

Fig. 16. Comparison between the discharge rate inside the reservoir Q_{in} and inside Q_{pipe} for both the configuration.

Fig. 17 shows the pressures acting on the OBREC cross sections. For both the configurations, the loads do increase with increasing H_s. The crown walls and the reservoirs are affected by impulsive impacts, while the ramp and the bottom edge of the device to the quasi static ones. For both the NW-LAB and the RS-LAB configurations, the most stressed part of the structure is the crown wall. Specifically, for the former the impacts are concentrated just above the pipe, while for the latter just below the bullnose. The higher ramp and the smaller reservoir generally increase the magnitude of the pressures against the crown wall, leading to a more stressed bullnose with respect to the NW-LAB cross section.

An integrated perspective shows a strong connection between the hydraulic and the structural performance. The highest waves overtop the ramp with more energy, which is partially dissipated in the direct impact against the crown wall. This dynamic does not allow a significant increase of Q_{pipe}

for the most severe sea states. The smallest waves, characterized by less energy, tend to follow the OBREC geometry flowing through the pipe without any loss.

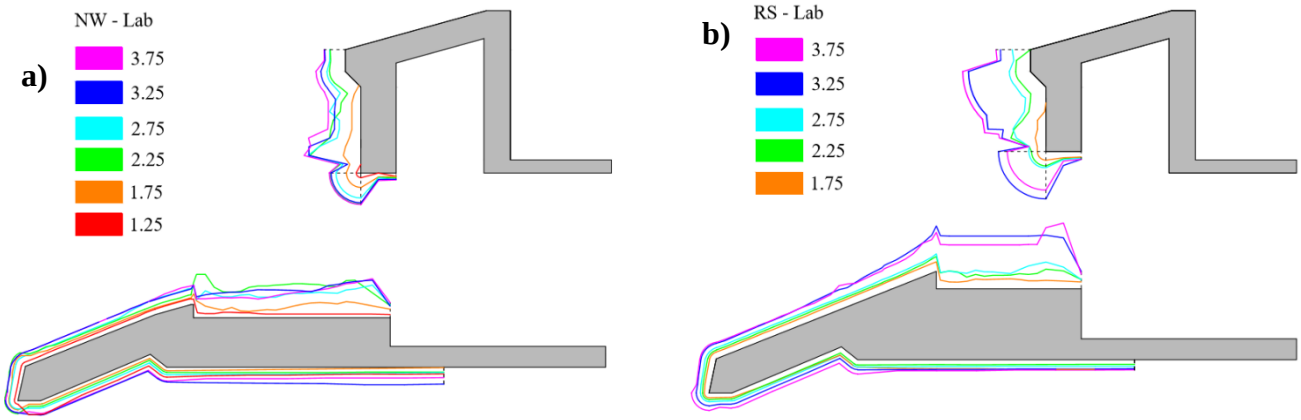

Fig. 17. Maximum values of pressures along the OBREC device: a) NW_LAB and b) RS_LAB configurations.

4.3 Scale effects on wave loads

During the small-scale OBREC experiments [12], the ramp was characterized by a quasi-static loading time history, while the crown wall was affected by signals showing evident rapid variations in time, with a high force peaks typically described as impact wave loads [12]. For the full-scale prototype, this is not completely true, at least for the ramp. In this latter case, the monitored pressure signals can be classified as slightly breaking and broken wave loads, due to the presence of the berm that anticipates the breaking process. The differences between the small and full-scale dynamics point out the strong non-linear interaction between the fluid and the ramp, in contrast with the quasi-static conditions measured during the laboratory campaigns [12,[**41**]. In particular, in correspondence of drastic changes of roughness and permeability, the air-water interface give some numerical disturbance leading to misleading results.

Furthermore, the qualitative analysis of the field measurements highlights that all the recorded signals are characterized by a strong noise including a significant number of negative values. The latter ones are due to the high-aeration occurring during the wave-structure interactions, which produces sub-atmospheric pressures after the impact takes place, as already observed in large-scale experiments [30].

However, the general hydrodynamic at prototype during extreme wave conditions was already well represented during the small-scale experiments [41]. In the laboratory, the creation of a “water bag” that attenuates the loads both on the reservoir and on the lower part of the crown wall was observed. At prototype scale, this process is confirmed by the pipe saturation occurred during the extreme events. Furthermore, the laboratory, the field and the numerical results highlight that the main difference between the RS-LAB and NW-LAB configurations is the point where the wave impact occurs. In case of the higher ramp the highest waves are conveyed directly towards the upper part of the crown wall, while in the lower one, the wave falls inside the reservoir and then run-up along the crown wall.

5. Theoretical power production

The purpose of this Section is to provide a preliminary assessment of the theoretical power flux available at prototype scale. The optimization of the cross section according to the results is also discussed.

5.1 Methodology

The assessment is based on hydraulic considerations disregarding the energy conversion method and the power losses. The theoretical power production is obtained by combining the overtopping rates flowing inside the shunt tank Q_{pipe} and the total hydraulic head h_{tot}, for each tested wave condition.
The hydrodynamics observed at the OBREC prototype, supported by the numerical modelling, showed that the overtopping waves are firstly collected inside the reservoir and then conveyed, by means of the pipe, in the machine room. Here, a shunt tank stabilizes the hydraulic head available for the hypothetical PTO system (Fig. 18a). The size of the tank installed in the OBREC prototype, i.e. 0.45 m (width) x 0.45 m (height) x 1 m (longitudinal extension), is showed in Fig. 18b. The most important parameter is the diameter of the hole on the bottom of the shunt tank, acting as intake for the turbine. As aforementioned, due to the limitation of the 2D model, the pipe toward the crown wall has been modeled as a rectangular hole covering the whole width of the domain. Therefore, the hydrodynamics inside the reservoir and the power efficiency parameters are computed by means of another specifically-designed numerical model, called OBRECsim [8]. OBRECsim solves the full, dynamic, 1-D Saint Venant equation using an implicit, finite difference method. The code is based on the continuity equation (2):

$$Q^*_{reservoir} = Q^*_{in} - Q^*_{rear} - Q^*_{overflow} \quad \textbf{(2)}$$

where: $Q^*_{reservoir}$ is the flow through the turbines; Q^*_{in} is the total overtopping flow rate, derived from the overtopping discharge formula fitted by Iuppa et al. [24] on the OBREC small-scale laboratory tests; Q^*_{rear} is the overtopping flow rate at the rear side of the structure; $Q^*_{overflow}$ is the outgoing reflected flow when the reservoir is saturated.

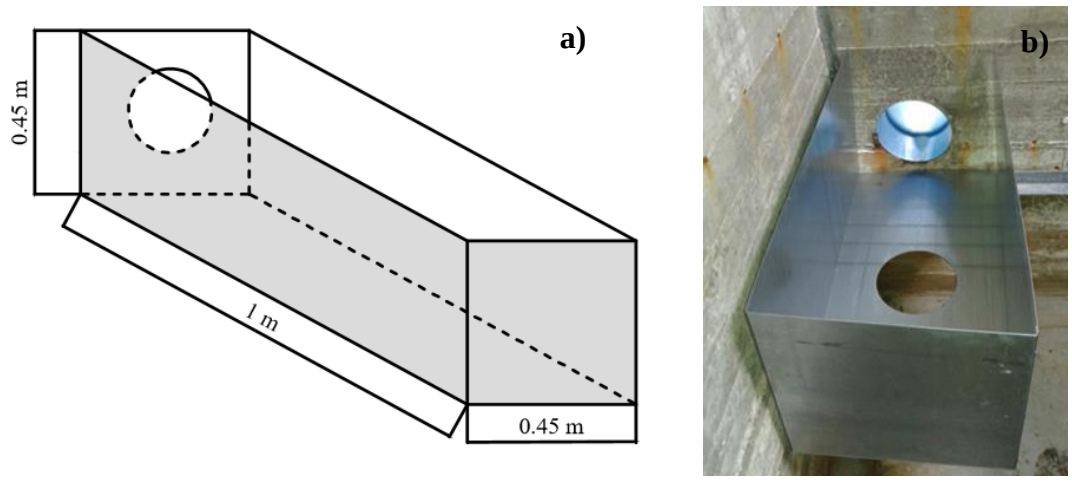

Fig. 18. Shunt tank: a) CAD scheme; b) installed in the prototype of the port of Naples.

The total hydraulic head h_{tot} is composed by 2 contributions (Eq. (3)), i.e. the difference between the still water level and the bottom edge of the reservoir h and the average hydraulic head dh established in the shunt tank (Fig. 18), dependent on Q_{pipe}:

$$h_{tot} = h + dh \quad \textbf{(3)}$$

where h is equal to 0.7 m and 1.25 m for the NW-LAB and RS-LAB sections, respectively. It is worthy to highlight that the value of dh represents only the static contribution, even if the observations pointed out the importance to consider also the kinetic one. Therefore, it represents a cautious assumption for the evaluation here performed.

The theoretical input power P_{in} to a generic Power Take Off (PTO) system, by neglecting the power losses, is given by:

$$P_{in,i} = \rho \cdot g \cdot Q_{pipe,i} \cdot h_{tot,i} \quad \textbf{(4)}$$

where ρ *is* the fluid density, g is the gravitational acceleration, h_{tot} is the total hydraulic head, Q_{pipe} is the overtopping discharge rate flowing through the pipe, and the subscript i is the sea state. The contribution given by each wave condition $E_{in,ws}$ (Table 7) is derived by multiplying the value obtained for a specific i for the frequency of occurrence Fr associated to i (in terms of hours/year). The sum of the values of $E_{in,ws}$ gives the theoretical available input power for the PTO system of each OBREC configuration during a year $E_{in,year}$.

5.2 Results

Table 6 shows the values of dh, P_{in}, $E_{in,ws}$ and the resultant $E_{in,year}$ for each OBREC configuration, according to the results obtained by the numerical modelling. Most of the sea states give values of dh (Table 7) greater than the height of the shunt tank, i.e. 0.45 m, and therefore the values of P_{in} is computed accounting for this upper limitation of dh. The shunt tank should be resized to allow a higher available hydraulic head and thus energy production.

For waves with H_s < 1.25 m, the NW-LAB configuration produces higher values of Q_{pipe} than the RS-LAB configuration (Table 6). The values of P_{in} for H_s =1.25 m are similar between the two configurations. For higher wave heights, P_{in} grows more and more for the RS-LAB cross section, highlighting that the smaller values of Q_{pipe} are effectively compensated by the higher values of h_{tot}, essentially due to the higher value of the constant contribution h.

It is worthy to remark that these results were derived in case of one hole and one corresponding 0.25 diameter pipe. The optimization of the design and location of the holes for the pipes requires a fully 3D modelling that is out of the scope of this contribution.

Table 7. Hydraulic head established in the shunt tank dh and power produced by the turbine P_{in}, for each sea state characterized by a certain frequency Fr and available theoretical power P_{year}. Values derived in case of one 0.25 m diameter hole.

Sea states			NW-LAB			RS-LAB		
H_s [m]	Fr [/]	P_{year} [kW/m]	dh [m]	P_{in} [kW]	$E_{in,ws}$ [kWh]	dh [m]	P_{in} [kW]	$E_{in,ws}$ [kWh]
0.25	0.1498	0.01	0.00	0.00	0.02	0.00	0.00	0.04

0.75	0.5912	0.60	0.01	0.16	842.02	0.00	0.08	427.74
1.25	0.2083	0.75	0.10	1.03	1886.72	0.05	1.00	1845.69
1.75	0.0409	0.34	0.20	2.09	751.62	0.16	2.74	983.72
2.25	0.0083	0.13	0.27	2.66	203.56	0.30	4.26	325.79
2.75	0.0012	0.03	0.31	2.93	25.63	0.40	5.13	44.96
3.25	0.0003	0.01	0.36	3.16	5.53	0.51	5.96	10.44
3.75	0.0001	0.00	0.37	3.12	2.19	0.54	5.82	4.08
Total	**1.00**	**1.87**			$E_{in,year}$ **3717.27**			$E_{in,year}$ **3642.46**

A coherent comparison between the two configurations can be performed by considering the values of $E_{in,year}$, which results to be 3717 kWh and 3642 kWh for the NW-LAB and RS-LAB cases, respectively. Being the total available wave energy of 4620 kWh/m, the Capture Width Ratio (CWR) is 12.9% and 12.6% for the NW-LAB and the RS-LAB, respectively. CWR is the percentage of the available wave power that is captured by the device per metre of device width. The lower ramp of NW-LAB captures a wider set of wave conditions, maximizing the OBREC operational window $T_{o.w.}$ with respect to the typical wave climate and P_{year} given the higher frequency of occurrence Fr of the less energetic sea states. The NW-LAB is characterised by an operational window $T_{o.w.}$ ($\sum Fr$) > 32% (Table 8), while the RS-LAB is able to operate just 10.3 % of the year.

The parameters $E_{in,year}$ and $T_{o.w}$ can be assumed as the reference parameters for the design optimisation of the ramp. However, appropriate site-specific threshold values for these parameters should be selected to derive the optimal value of R_c, while considering the design procedure and the technical considerations here reported of general validity.

The theoretical results of the power production have finally to cope with the technical characteristics of the selected PTO. The very low head turbines tested for OBREC can exploit minimum head differences ≥1.5m [44], and therefore the NW-LAB configuration would not produce energy, while the RS-LAB configuration would produce energy only for the highest waves (see Table 8). Therefore, the final design of the device has to account for the limitations of the PTO system, which in this specific case does not allow the selection of the NW-LAB configuration. These considerations point out, once more, that the very low head turbine is still a challenge to be overcome (Contestabile et al., 2020), and that improved technological solutions have to be developed to make feasible the systematic production of marine renewable energy.

Table 8. Yearly operating time, in terms of percentage per year, and total average hydraulic heads $dh_{tot,real}$ computed for each sea state.

		NW-LAB		RS-LAB	
#	H_{m0} **[m]**	$T_{o.w.}$ **[%]**	$h_{tot,real}$ **[m]**	$T_{o.w.}$ **[%]**	$h_{tot,real}$ **[m]**
1	0.25	0.00	0.70	0.00	1.25
2	0.75	12.92	0.71	1.71	1.25
3	1.25	14.63	0.80	5.50	1.30
4	1.75	3.79	0.90	2.33	1.41
5	2.25	0.85	0.97	0.67	1.55
6	2.75	0.10	1.01	0.09	1.65
7	3.25	0.02	1.06	0.02	1.76
8	3.75	0.01	1.07	0.01	1.79

Total	32.32	/	10.34	/

5.3 Cross section optimization for energy production

The results obtained from the analysis reported in Section 0 could be useful to give some indications about the optimal design of the OBREC device, in order to maximize the energy production.

According to its principle of operation, the main design parameter is the height of the ramp R_c, which determines the run-up process, and therefore the overtopping rate. Its definition can be independent from the reservoir width, which has to primarily satisfy the site-specific constraints related to i) the available space for the overall structure, and consequently ii) the construction and the installation costs. An undersized reservoir, with respect to the highest overtopping volumes, allows the dissipation of part of the wave energy during the wave-crown wall impact, protecting the machine room that contains sensitive instruments. Therefore, the selection of the reservoir width has to be subordinated to the value of R_c and to the related estimate of the overtopping volumes.

For the specific case of the prototype installation, the lower ramp maximizes the theoretical power available to the system, being capable of exploiting a wider range of wave conditions with respect to the higher ramp. However, the selection of the proper value of R_c, during the design procedure, cannot be independent from the minimum hydraulic head needed for the selected PTO system to produce energy.

6. Conclusions

The general aim of this contribution is to carry-out an integrated assessment of the OBREC prototype installed in the port of Naples, in terms of its hydraulic and structural performance. The OBREC consists of a ramp followed by a unique reservoir closed by a crown wall, provided with a bullnose on top of it. The reservoir is located above the still water level and it is linked with the machine room by means of a pipe passing through the crown wall. Specifically, the prototype is composed by two cross sections, which differ mainly for the height of the ramp. The lower one (NW-LAB) is aimed to capture the most frequent waves, while the higher (RS-LAB) the highest ones.

The OBREC performance is analysed by combining the field measurements, gathered at the installation site, and the numerical modelling performed in the openFOAM environment. The calibration of the numerical model is based on the pressures monitored during a real storm event. The OBREC cross sections were tested in 2D conditions, considering that the principal direction of the wave propagation, in the Gulf of Naples, is orthogonal to the device. Under extreme events, two cross section profiles were modelled for both NW-LAB and RS-LAB: an “open” and a “closed” profile, which include (real case) or not the presence of the pipe, respectively, to represent the case of pipe saturation observed.

The numerical model tends to generally overestimate the field data, except for the upper part of the crown wall of the open configuration, probably due to the presence of the rectangular section covering the width. Therefore, the monitored maximum pressures fall in the middle of these two cases, i.e. open and closed reservoirs. The numerical values of p_{250} (non-exceedance level of 99.7%) show a good agreement with the field measurements at the wall, while strongly overestimate the stresses along the ramp. This could be due to the curved offshore profile of the real breakwater that slightly anticipates the breaking process, which is not reproduced in the virtual domain. Furthermore, some numerical mesh limitations lead to a different air-water interface under the ramp element.

The numerical model is then adopted to test the prototype under the typical wave climate of Naples. The results obtained show that OBREC is capable of minimizing the overtopping discharge at the rear side of the structure, without increasing the wave reflection.

The theoretical power available to the PTO system in a year, i.e. $E_{in,year}$, is derived by combining the overtopping rates flowing inside the shunt tank Q_{pipe} and the total hydraulic head h_{tot}, for each tested wave condition, accounting for the frequency of occurrence *Fr* associated to each sea state. The values of $E_{in,year}$, in case of only one 0.25 m diameter hole, are equal to 3717.27 kWh and 3642.46 kWh for the NW-LAB and RS-LAB, corresponding to CWR of 12.9% and 12.6%, respectively.

Indeed, the lower ramp captures a wider set of wave conditions characterized by an operational window $T_{o.w.}$ > 32%, while for the RS-LAB the values of $T_{o.w.}$ resulted to be > 10%. These two parameters are crucial for the design optimisation of the ramp, even if site-specific threshold values should be selected. The hydraulic optimization has finally to be combined with the technical characteristics, and sometimes the limitations, of the available PTO systems. For the case of OBREC, the selection of commercial low-head turbines implies that the NW-LAB configuration cannot be selected because of the insufficient hydraulic head for turbine operation.

Acknowledgments

The support of the European Commission through the H2020 project BRIGAID "Bridging the gap for innovations in disaster resilience "is gratefully acknowledged. The support of the University of Campania "Luigi Vanvitelli" through the VALERE program (VAnviteLli pEr la RicErca, 2017) is gratefully acknowledged. The authors acknowledge the University of Bologna for encouraging the mobility of researchers.

References

[1] Azzellino, A., Lanfredi, C, Contestabile, P., Ferrante, V., & Vicinanza, D. (2011). Strategic environmental assessment to evaluate WEC projects in the perspective of the environmental cost-benefit analysis. In Proceedings of the Twenty-First International Offshore and Polar Engineering Conference, Maui, HI, USA, 19–24 June 2011.

[2] Boake, C., B., Whittaker, T., J., Folley, M., & Ellen, H. (2002). Overview and initial operational experience of the LIMPET wave energy plant. In Proceedings of the Twelfth International Offshore and Polar Engineering Conference, Kitakyushu, Japan, 26–31, 27.

[3] Boccotti, P. (2007). Caisson breakwaters embodying an OWC with a small opening–Part I: Theory. Ocean Eng., 34, 806–819. 25.

[4] Bouma, T., J., Van Belzen, J., Balke, T., Zhu, Z., Airoldi, L., Blight, A., J. & Lara, J., L. (2014). Identifying knowledge gaps hampering application of intertidal habitats in coastal protection: Opportunities & steps to take. Coastal Engineering, 87, 147-157.

[5] Buccino, M., Dentale, F., Salerno, D., Contestabile, P., & Calabrese, M. (2016). The use of CFD in the analysis of wave loadings acting on seawave slot-cone generators. Sustainability, 8(12), 1255.

[6] Centurioni, L., Braasch, L., Di Lauro, E., Contestabile, P., De Leo, F., Casotti, R., Franco, L., & Vicinanza, D. (2017). A new strategic wave measurement station off Naples port main breakwater. Coast. Eng. Proc. 1, 36.

[7] Christensen D., E., & Deigaard, R. (2001). Large eddy simulation of breaking waves. Coastal Engineering, Volume 42, Issue 1, 2001, Pages 53-86.
[8] Contestabile, P., & Vicinanza, D. (2018). Coastal Defence Integrating Wave-Energy-Based Desalination: A Case Study in Madagascar. Journal of Marine Science and Engineering, 6(2), 64.
[9] Contestabile, P., Aristodemo, F., Vicinanza, D., & Ciavola, P. (2012). Laboratory study on a beach drainage system. Coast. Eng., 66, 50–64.
[10] Contestabile, P., Ferrante, V., Di Lauro, E., & Vicinanza, D. (2016). Prototype Overtopping Breakwater for Wave Energy Conversion at Port of Naples. In Proceedings of the 26th International Conference ISOPE, Rhodes, Greece, 616–621.
[11] Contestabile, P., Ferrante, V., Di Lauro, E., & Vicinanza, D. (2017b). Full-scale prototype of an overtopping breakwater for wave energy conversion. Coastal Engineering Proceedings, 1(35), 12.
[12] Contestabile, P., Iuppa, C., Di Lauro, E., Cavallaro, L., Andersen, T. L., & Vicinanza, D. (2017a). Wave loadings acting on innovative rubble mound breakwater for overtopping wave energy conversion. Coast. Eng., vol. 122, pp. 60-74.
[13] Contestabile, P., Lauro, E. D., Galli, P., Corselli, C., & Vicinanza, D. (2017c). Offshore wind and wave energy assessment around Malè and Magoodhoo Island (Maldives). Sustainability, 9(4), 613.
[14] Dafforn, K., A., Glasby, T., M., Airoldi, L., Rivero, N., K., Mayer-Pinto, M., & Johnston, E., L. (2015). Marine urbanization: an ecological framework for designing multifunctional artificial structures. Frontiers in Ecology and the Environment, 13(2), 82-90.
[15] Di Lauro, E., Lara, J. L., Maza, M., Losada, I. J., Contestabile, P., & Vicinanza, D. (2019). Stability analysis of a non-conventional breakwater for wave energy conversion. Coastal Engineering, 145, 36-52.
[16] Di Lauro, E., Maza, M., Lara, J.L., Contestabile, P., Losada, I.J. & Vicinanza, D. (2017). Numerical analysis of a nonconventional breakwater for wave energy conversion. Proceedings of the 8th SCACR—International Short Conference on Applied Coastal Research, Santander, Spain, 2017.
[17] Doody, J. P. (2008). Saltmarsh conservation, management and restoration (Vol. 12). Springer Science & Business Media.
[18] Eurotop. 2016. In: Pullen, T., Allsop, N.W.H., Bruce, T., Kortenhaus, A., Schüttrumpf, H., & van der Meer, J.W. (Eds.), Wave Overtopping of Sea Defences and Related Structures – Assessment Manual. www.overtopping-manual.com.
[19] Forchheimer, P. 1901. Wasserbewegung durch Boden. Zeitschrift des Vereines Deutscher Ingenieuer, 45 edition.
[20] Formentin, S. M., Palma, G., Contestabile, P., Vicinanza, D. & Zanuttigh, B. (2017). 2DV RANS-VOF numerical modeling of a multifunctional harbor structure. Coast. Eng. Proc., 1, 3.
[21] Geuzaine, C. & Remacle, J.-F. (2009). Gmsh: A 3-D finite element mesh generator with built-in pre- and post-processing facilities. Int. J. Numer. Meth. Engng., 79: 1309–1331.
[22] Hanley, M. E., Hoggart, S. P. G., Simmonds, D. J., Bichot, A., Colangelo, M. A., Bozzeda, F. & Trude, R. (2014). Shifting sands? Coastal protection by sand banks, beaches and dunes. Coastal Engineering, 87, 136-146.
[23] Hinkel, J., Lincke, D., Vafeidis, A. T., Perrette, M., Nicholls, R. J., Tol, R. S.J., Levermann, A. (2014). Coastal flood damage and adaptationcosts under 21st century sea-level rise. Proceedings of the National Academy of Sciences, 111, 3292–3297.
[24] Iuppa C., Contestabile, P., Cavallaro, L., Foti, E. & Vicinanza, D. (2016). Hydraulic performance of an innovative breakwater for overtopping wave energy conversion. Sustainability, vol. 8, pp. 1226.
[25] Jacobsen, N.G., Fuhrman, D.R., & Fredsoe, J. (2012). A wave generation toolbox for the open-source CFD library: OpenFoam Int. J. Numer. Methods Fluids, 70. pp. 1073-1088.
[26] Jensen B., Jacobsen N. G., & Christensen, E. D. (2014). Investigations on the porous media equations and resistance coefficients for coastal structures. Coastal Engineering, Volume 84, Pages 56-72.

[27] Mansard, E.P.; Funke, E.R. The measurement of incident and reflected spectra using a least squares method. In Coastal Engineering 1980; American Society of Civil Engineers: Reston, VA, USA, 1980; pp. 154–172.
[28] Mendoza, E., Silva, R., Zanuttigh, B., Angelelli, E., Andersen, T. L., Martinelli, L., & Ruol, P. (2014). Beach response to wave energy converter farms acting as coastal defence. Coastal Engineering, 87, 97-111.
[29] Ondiviela, B., Losada, I. J., Lara, J. L., Maza, M., Galván, C., Bouma, T. J., & van Belzen, J. (2014). The role of seagrasses in coastal protection in a changing climate. Coastal Engineering, 87, 158-168.
[30] Oumeraci H., Kortenhaus, A., Allsop, W., de Groot, M., Crouch, R., Vrijling H., & Voortman H. (2001). Probabilistic design tools for vertical breakwaters. CRC Press.
[31] Palma G., Contestabile, P., Formentin, S. M., Vicinanza, D. & Zanuttigh, B. (2016). Design optimization of a multifunctional wave energy device. In Progress in Renewable Energies Offshore, Proc. of the 2nd International Conference on Renewable Energies Offshore (RENEW2016), Lisbon, Portugal, 24–26 October.
[32] Palma G., Formentin, S. M., Zanuttigh, B., Contestabile, P. & Vicinanza, D. (2019). Numerical Simulations of the Hydraulic Performance of a Breakwater-Integrated Overtopping Wave Energy Converter," Journal of Marine Science and Engineering, 7(2), 38.
[33] Pecher, A., Kofoed, J.P., Le Crom, I., Neumann, F. & Azevedo, E., D., B. (2011). Performance assessment of the Pico OWC power plant following the EquiMar Methodology. In Proceedings of the Twenty-First International Offshore and Polar Engineering Conference, Maui, HI, USA, 19–24 June. 26.
[34] Rendle, E. J., & Rodwell, L. D. (2014). Artificial surf reefs: A preliminary assessment of the potential to enhance a coastal economy. Marine Policy, 45, 349-358.
[35] Romano, A., Bellotti, G., Briganti, R., & Franco, L. (2014). Uncertainties in the physical modelling of the wave overtopping over a rubble mound breakwater: the role of the seeding number and of the test duration. Coastal Eng., 103, 15–21.
[36] Stive, M., J., de Schipper, M., A., Luijendijk, A., P., Aarninkhof, S., G., van Gelder-Maas, C., van Thiel de Vries, J., S., ... & Ranasinghe, R. (2013). A new alternative to saving our beaches from sea-level rise: The sand engine. Journal of Coastal Research, 29(5), 1001-1008.
[37] Torre-Enciso, Y., Ortubia, I., López de Aguileta, L., I., Marqués, J. (2009). Mutriku wave power plant: from the thinking out to the reality. In: Proceedings 8th European Wave Tidal Energy Conference, 319–29.
[38] Van Doorslaer, K., & De Rouck, J. (2010). Reduction on Wave Overtopping on a Smooth Dike by Means of a Parapet. Proceedings of the 32nd International Conference on Coastal Engineering 2010, Shanghai, China.
[39] Van Doorslaer, K., De Rouck, J., Audenaert, S., & Duquet, V. (2015). Crest modifications to reduce wave overtopping of non-breaking waves over a smooth dike slope. Coast. Eng., 101, 69–88.
[40] Van Gent, M. R. A. (1995). Porous flow through rubble-mound material. Journal of waterway, port, coastal, and ocean engineering, 176-181.
[41] Vicinanza, D., Contestabile, P., Harck Nørgaard, J., & Lykke Andersen, T. (2014). Innovative rubble mound breakwaters for overtopping wave energy conversion. Coastal Eng., 88, 154–170.
[42] Vicinanza, D., Di Lauro, E., Contestabile, P., Gisonni, C., Lara, J. L., & Losada, I. J. (2019). Review of Innovative Harbor Breakwaters for Wave-Energy Conversion (Doctoral dissertation, American Society of Civil Engineers).
[43] Vicinanza, D., & Frigaard, P. (2008). Wave pressure acting on a seawave slot-cone generator. Coast. Eng., 55, 553–568.
[44] VLH Turbine. Available online: http://www.vlh-turbine.com/products/vlh-turbine/ (accessed on 30 November 2019).

[45] Zanuttigh, B., Nicholls, R., J., Vanderlinden, J., P., Thompson, R., C., & Burcharth, H., F. (Eds.). (2014). Coastal risk management in a changing climate. Butterworth-Heinemann.
[46] Zhiyin, Y. (2015). Large-eddy simulation: Past, present and the future. Chinese journal of Aeronautics, 28(1), 11-24.